Cement and Concrete Composites 170 (2026) 106591

Contents lists available at ScienceDirect

Cement and Concrete Composites

journal homepage: www.elsevier.com/locate/cemconcomp

Pull-out mechanism of striated steel fibers in ultra-high performance concrete (UHPC): Experimental study and analytical modeling

Sukhoon Pyo [a,b,*], Zhengye Tang [a], Min-Chun Han [a], Sherif El-Tawil [a]

[a] Department of Civil & Environmental Engineering, University of Michigan, 2350 Hayward, G.G. Brown, Ann Arbor, MI, 48109-2125, USA
[b] Department of Civil, Urban, Earth, and Environmental Engineering, Ulsan National Institute of Science and Technology (UNIST), 50 UNIST-gil, Ulju-gun, Ulsan, 44919, Republic of Korea

ARTICLE INFO

Keywords:
Striated steel fiber
Fiber pull-out
Analytical model
Ultra-high performance concrete (UHPC)
Fiber anchoring mechanism

ABSTRACT

This study presents the first mechanistic investigation of striated steel fibers, a newly developed fiber type optimized for ultra-high performance concrete (UHPC). Through single-fiber pull-out experiments and finite element (FE) simulations, the research examines the interfacial mechanisms governing load transfer between striated fibers and UHPC. The striated fibers, featuring micrometer-scale surface depressions, exhibit a distinctive multistage pull-out response marked by alternating load rises and drops, which correspond to successive engagement and release of the striations. This behavior, not observed in conventional deformed or smooth fibers, reflects a unique combination of adhesion, frictional sliding, and mechanical interlocking within the dense UHPC matrix. On average, the striated fibers achieved 104% higher maximum pull-out load and 126% greater equivalent bond strength than smooth fibers, attributed to the formation of localized shear keys and enhanced frictional resistance. Detailed computational simulation captured the evolution of these anchorage-sliding cycles and clarified the local crushing and reanchoring of the matrix around each striation. An analytical model was also developed to represent both the frictional and anchorage contributions to pull-out resistance. The findings provide the first direct experimental and numerical evidence of the progressive bond mechanisms in striated fibers and establish a mechanistic foundation for optimizing their geometry and application in next-generation UHPC systems.

1. Introduction and motivation

The mechanical performance of high-performance fiber-reinforced cementitious composites depends on the quality of the interfacial bond between fibers and the surrounding matrix. During crack opening, this bond governs the efficiency of stress transfer from the matrix to the fibers, directly influencing the composite's tensile strength, crack resistance, and energy dissipation capacity [1]. Fiber pull-out tests provide a direct method for evaluating the bond characteristics between fibers and their surrounding matrix. Numerous studies using this technique have shown that bond capacity is influenced by factors such as fiber geometry, matrix strength, and embedment length [2,3].

The pull-out resistance of steel fibers in concrete depends largely on fiber design. Straight steel fibers with smooth surfaces primarily depend on chemical adhesion and interfacial friction with the matrix for resistance. Enhancing matrix density or fiber surface roughness can increase the peak pull-out load for these fibers, while extending embedment length improves energy absorption [4,5]. However, the basic design of straight fibers limits opportunities for significant performance innovation, aside from basic surface modifications such as mechanical or chemical roughening [6,7].

In response, recent studies have explored micro-texturing and surface modification strategies to enhance the bond performance of steel fibers in UHPC. Chemical and nano-scale surface treatments, including calcium carbonate precipitation, silane coupling agents, and hybrid nano-coatings, have been shown to improve fiber-matrix bonding by increasing surface roughness, promoting chemical adhesion, and densifying the interfacial transition zone (ITZ) [8–11]. These approaches primarily enhance pull-out resistance through modified interfacial chemistry and microstructural refinement, leading to increased bond strength and pull-out energy. While effective, such methods rely on additional processing steps, raise concerns regarding coating durability, and require chemical compatibility with the matrix, which may influence scalability and long-term performance.

* Corresponding author. Department of Civil & Environmental Engineering, University of Michigan, 2350 Hayward, G.G. Brown, Ann Arbor, MI, 48109-2125, USA.
E-mail address: shpyo@unist.ac.kr (S. Pyo).

https://doi.org/10.1016/j.cemconcomp.2026.106591
Received 22 October 2025; Received in revised form 6 March 2026; Accepted 19 March 2026
Available online 19 March 2026

In contrast to surface-modified fibers, research has also focused on introducing geometric deformations to maximize mechanical interlocking and pull-out resistance, thus reducing the required fiber dosage. Deformed fibers, including hooked-end, indented, crimped, wavy, polygonal twisted, and spiral types, rely primarily on anchorage mechanisms created by their shapes [12]. For instance, hooked-end fibers resist pull-out through plastic unbending of their hooks, while twisted fibers mobilize mechanical interlock along their entire length, offering higher bond strength and a slip-hardening response compared to traditional designs [3,13–16].

Striated steel fibers are a new type of steel fibers recently introduced by El-Tawil [17]. The fibers are optimized for use in ultra-high performance concrete (UHPC) and employ micrometer-scale surface striations that facilitate the formation of shear keys to boost adhesion, friction and anchorage mechanisms in UHPC [18]. El-Tawil [17] demonstrated that, compared to traditional straight steel fibers commonly used in UHPC, these improvements enable either substantially greater ductility at the typical 2% by volume dosage or comparable performance at reduced fiber content, providing significant economic advantages. For example, El-Tawil et al. [19] utilized the fibers at a dosage of 1.5% in the construction of a UHPC bridge in the United States. The resulting field-cast UHPC exhibited adequate strain-hardening behavior per the new AASHTO Guide Specification for UHPC [20]. Despite their commercial availability and application, the load-transfer mechanisms governing the behavior of striated fibers remain largely unexplored and are the object of this research.

This paper seeks to develop an understanding of the performance of striated steel fibers through experimentation, finite element (FE) simulation, and analytical modeling. Focusing on pull-out performance, the study elucidates the progressive stages of performance, ranging from fully bonded to debonding, shear key anchorage in the striations, frictional sliding, and re-anchorage, which govern the behavior of striated steel fibers embedded in UHPC. The resulting insights aim to guide the optimization of matrix composition, striation geometry, and embedment length for next-generation steel fiber-reinforced UHPC applications.

2. Experimental program

2.1. Mixing and specimen preparation

An open-source UHPC mix developed by El-Tawil et al. [21] was adopted for this study. This mixture, which costs only a fraction of proprietary UHPC formulations, was chosen for its practicality, performance, and the ability to easily source its components from commercial suppliers. The mix proportion of the UHPC constituents is listed in Table 1. Two grades of quartz silica sand were incorporated, with maximum particle sizes of 200 μm and 800 μm, respectively. Table 2 summarizes the geometric characteristics of the two types of straight, brass-coated, steel fibers used in this study: striated fibers and comparable straight, smooth steel fibers against which the striated fiber's performance is measured. Fig. 1 presents an SEM image of the striated fiber, showing the longitudinal striations spaced at approximately 370 μm intervals. In contrast, the smooth fiber has a plain surface finish.

Mixing was performed for approximately 20 min using a 40-L rotating pan mixer. The measured spread of the fresh UHPC (without steel fibers) was 257 mm. Several types of specimens were made, including compression cubes, tensile coupons, and half-dogbone pullout specimens. In making the pullout specimens, a steel fiber was precisely positioned within each half-dogbone mold to achieve an embedded length of 5 mm before casting. The freshly prepared UHPC (without fibers) was cast from the center of the half-dogbone molds, allowing the material to flow and fill all four corners due to its inherent high workability. Once the pullout specimens were made, steel fibers were then added to the mix at the specified dosage, and the remaining specimens (cubes and coupons) were prepared after additional mixing. Following casting, the specimens were covered with plastic sheets and maintained at room temperature for 24 h to prevent moisture loss. The hardened specimens were then demolded and subjected to accelerated curing by immersion in a water bath at 90 °C for 48 h. All mechanical tests were conducted about 7 days after casting. The compressive strength of the UHPC reinforced with striated steel fibers (1.5% by volume) was 191.6 MPa. Additional details on the UHPC's compressive strength and tensile performance, including its strain hardening response, can be found in Tang et al. [18].

Table 1
Mixture proportions by weight.

Materials	Ratio
Cement	0.50
Ground Granulated Blast-furnace Slag (GGBS)	0.50
Silica Fume	0.25
Water	0.22
Superplasticizer	0.005
Sand[a]	1.31

[a] The weight ratio of finer sand to coarser sand is 1:4.

Table 2
Properties of steel fibers used in this study.

Notation	Diameter d_f (mm)	Length l_f (mm)	Tensile strength MPa (ksi)	Elastic modulus MPa (ksi)
Smooth	0.2	13	2670 (387)	200000 (29000)
Striated	0.2[a]	13	2930 (425)	202000 (29300)

[a] Nominal diameter d_f.

2.2. Single fiber pull-out test procedure

Single fiber pull-out tests were performed on 13 mm-long striated and smooth fibers using an MTS Landmark® Servohydraulic test system, model 370.10. Load was measured using an MTS Acumen Tandem Load Cell Kit with a capacity of 0.100klbs (445N). All tests were performed at a constant pull-out rate of 0.0167 mm/s. Fig. 2(a) and (b) show the single fiber pull-out test setup and the specimen geometry, respectively. The pulled-out fibers were examined using the secondary electron (SE) detector of a TESCAN MIRA3 field-emission scanning electron microscope (FEG-SEM), operated at a beam intensity of 10 nA and an accelerating voltage of 20 kV. No sample preparation was performed to preserve the native damage mechanisms. The fiber samples were mounted on SEM stubs using carbon tape.

The pull-out energy was calculated as the area under the pull-out stress–slip curve, where the pull-out stress refers to the tensile stress induced in the fiber by the applied load. This area was integrated up to the point of complete fiber extraction. Additionally, the equivalent bond strength was determined from the same curve, as defined by Kim et al. [13] and Wille and Naaman [22], and is expressed in Eq. (1):

$$\tau_{eq} = \frac{pullout\ energy \times d_f}{L_E^2} \tag{1}$$

where d_f is the fiber diameter and L_E is the initial embedment length. The equivalent bond stress reflects a uniform interfacial stress distributed over the embedment length and is linearly related to the pull-out energy. In addition, the average bond strength, derived from the maximum pull-out load (P_{max}) and the initial embedment length, can be estimated using the approach proposed by Wille and Naaman [22], as shown in Eq. (2):

$$\tau_{av} = \frac{P_{max}}{\pi \times d_f \times L_E} \tag{2}$$

3. Experimental results and discussion

Fig. 3 presents the pull-out load and corresponding fiber stress–slip relationships for both fiber types. The straight smooth steel fibers

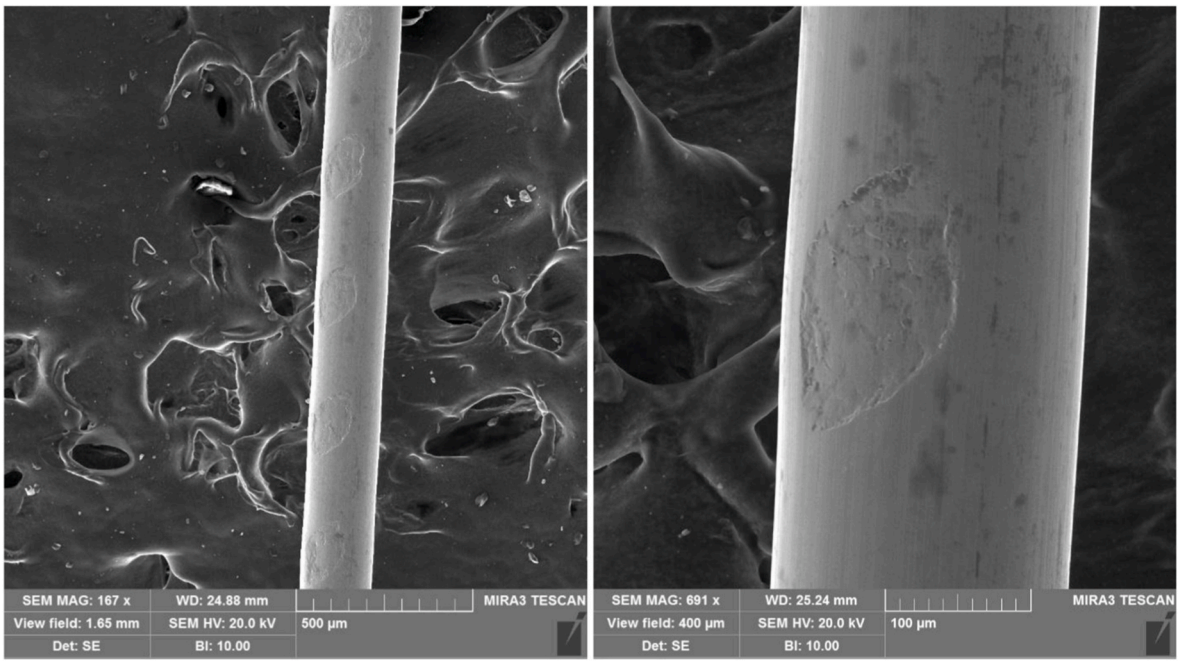

Fig. 1. Microscopic image of the striated steel fiber.

exhibited a rapid load drop after reaching the peak, which is attributed to the sudden loss of adhesion, followed by a more gradual loss of resistance with increasing pullout (Fig. 3(a)). The latter phase is attributed to the sustained frictional resistance at the fiber–matrix interface associated with the high packing density of the UHPC matrix around the fiber [23]. A striking contrast emerges between Fig. 3(a) and (b) where the striated fibers (in the latter figure) exhibit a repetitive pattern of load increases and decreases, in contrast to the smooth fiber's mostly monotonically decreasing response. Thirteen load peaks are observed for the striated fiber, which corresponds to the number of striations along the embedded length., i.e. each striation is responsible for a full wave of the force-slip response. This type of behavior has not been observed in any of the existing deformed steel fibers.

Table 3 summarizes the pull-out load, pull-out energy, and equivalent bond strength. The striated fiber achieves, on average, 104% higher pull-out load and 126% higher equivalent bond strength compared to the smooth fiber.

Microscopic observations provide insight into the reasons for the enhanced performance of striated fibers compared to smooth fibers. Significant surface damage is evident on both types of brass-coated steel fibers, as shown in Figs. 4 and 5. The brass coating is visibly worn and deeply scratched in the longitudinal direction, indicating abrasive interaction with the matrix. In the case of the striated fibers, UHPC residue is consistently found retained within each striation after testing (Fig. 4), while only minimal UHPC debris appears on the surface of the smooth fiber (Fig. 5). The deep longitudinal scratches, like those seen on the smooth fibers, are observed to continue across the striations, implying that each shear key squeezed past the striation in which it was embedded. The UHPC debris deposited in the striations suggests that the shear keys sustained damage as they moved across the striation, further contributing to the resistance mechanisms. In essence, each rising part of the force-slip response is associated with the shear keys squeezing past their striation and the low point is associated with the shear keys settling into the following set of striations as the fiber is pulled out. These observations help explain the unique load-slip pattern observed for the striated fiber compared to the smooth steel fiber and other types of deformed steel fibers. Additional insights into the performance of the striated fibers is gleaned from detailed finite element analysis presented later in the paper and then used to formulate an analytical model.

4. Computational simulation of fiber pull out process

Finite element modeling was conducted using the LS-DYNA explicit solver (R13.1, double precision) to gain qualitative insight into the complex pullout behavior exhibited by striated fibers. To facilitate model development and interpretation, the problem was idealized as axisymmetric, even though the striations are present only on two opposing sides of the fiber rather than around its full circumference. The finite element model and applied boundary conditions are shown in Fig. 6.

The UHPC domain was modeled with dimensions 100 times larger than those of the steel fiber to minimize boundary effects. Because the striation geometry could not be fully resolved from SEM images, the striation depth was estimated as 2.5 µm based on the available micrographs, while the side taper length and bottom length were assumed to be 15 µm and 140 µm, respectively, as illustrated in Fig. 6. The center-to-center spacing between successive striations was 370 µm. Consistent with experimental observations, a total of 13 striations were modeled along a fiber length of 4810 µm.

The model was formulated as an elastic representation of the fiber–matrix interaction and is therefore not intended to provide quantitative agreement with experimental pullout forces. Incorporation of nonlinear damage, plasticity, evolving contact conditions and debris formation in the UHPC would be required for improved quantitative prediction and is identified as a topic for future work.

The model was discretized using axisymmetric solid elements (ELFORM 15 shell sections) and the finest elements were about 2.5 µm to capture local effects. The centroidal axis of the fiber served as the axis of symmetry, corresponding to the y-axis direction in Fig. 6. Roller boundary conditions were applied along the axis of symmetry and on the right and bottom boundaries of the UHPC domain. The fiber pull-out process was simulated by applying displacement control along the y-direction through prescribed motion on the top nodes of the fiber, as illustrated in Fig. 6. To reduce running time to a reasonable value, a maximum displacement of 1200 µm was imposed. This value corresponded to pull-out of at least three striations.

LS-DYNA's contact keyword CONTACT_2D_AUTOMATIC_SINGLE_SURFACE was used to simulate the friction between the UHPC and the fiber. Both static and dynamic coefficients were assumed as 0.375

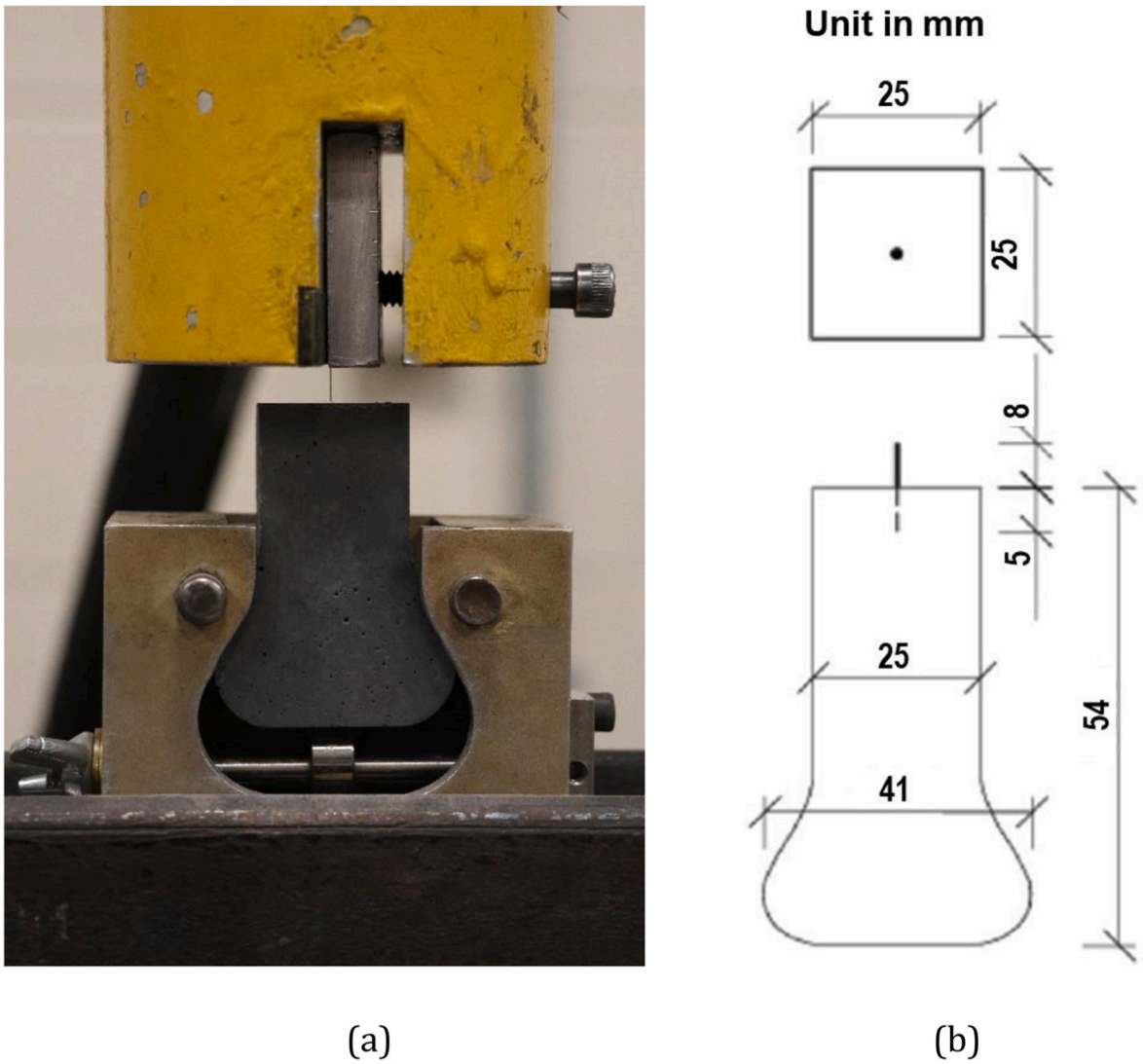

Fig. 2. (a) Single fiber pull-out test setup; (b) specimen geometry.

with a penalty force stiffness scale factor (SFACT) of 2 to ensure stable contact between the two materials. The steel fiber was modeled as a rigid body using elastic material (MAT_001) with an elastic modulus of 2020 GPa, which is 10 times its actual value as presented in Table 2, and a Poisson's ratio of 0.3. In the absence of sufficient information to define plasticity and damage behavior (for example, high confinement, crushing, and debris formation), the UHPC matrix was idealized as a linear elastic material (MAT_001) with an elastic modulus of 45 GPa and a Poisson's ratio of 0.2, following Graybeal [24].

Fig. 7(a) presents the load–slip curves from the FE model. The SAE filter was applied to the load histories obtained through FE modeling with a time unit of microseconds and a C/s range of 20 Hz to remove high-frequency noise for both fibers. An additional SAE filter, with a time unit of milliseconds and a C/s range of 10 Hz, was applied to smooth the curve. The predicted pullout load is substantially higher than the experimental results due to the use of a linear elastic model for the UHPC matrix. As discussed next, the model provides a unique qualitative explanation of the sawtooth nature of the pullout process observed in the tests.

Fig. 7(b) links the applied loading to key stages of the fiber sliding process. As load is applied, the striations engage the UHPC extrusions at the fiber–matrix interface, causing a rapid increase in resistance. The pullout force reaches a maximum ($\boldsymbol{P_{max}}$, shown in Fig. 7(a)) when the striations slide past the UHPC extrusions, leaving the striation cavities temporarily unfilled (see the "gap" in Fig. 7(b)). The resistance then decreases as the UHPC extrusions gradually seat back into the subsequent set of striations. Because one striation segment (370 μm, corresponding to approximately 1/13 of the fiber length) is mobilized per loading cycle (Point C in Fig. 7(b)), the peak force in each successive cycle is reduced by roughly $\boldsymbol{P_{max}}/13$, as reflected in Fig. 7(a). The model results provide qualitative insight into the observed sawtooth pullout response of striated fibers, which is further discussed in the next section.

5. Analytical modeling of fiber pull out response

5.1. Fiber pull-out mechanisms

Using the knowledge gained from the experiments and simulations, the responses of both types of fibers can be divided into distinct stages that correspond to the interfacial mechanisms governing load transfer and slip progression. These stages are discussed in detail next.

5.1.1. Straight smooth steel fiber

The pull-out response of the straight, smooth steel fibers generally occurs in three distinct stages, as outlined by Zhan and Meschke [25]. At low slip levels, the fiber-matrix interface is governed by chemical adhesion, resulting in a fully bonded interface and a nearly linear load–slip relationship. As slip increases, progressive debonding reduces

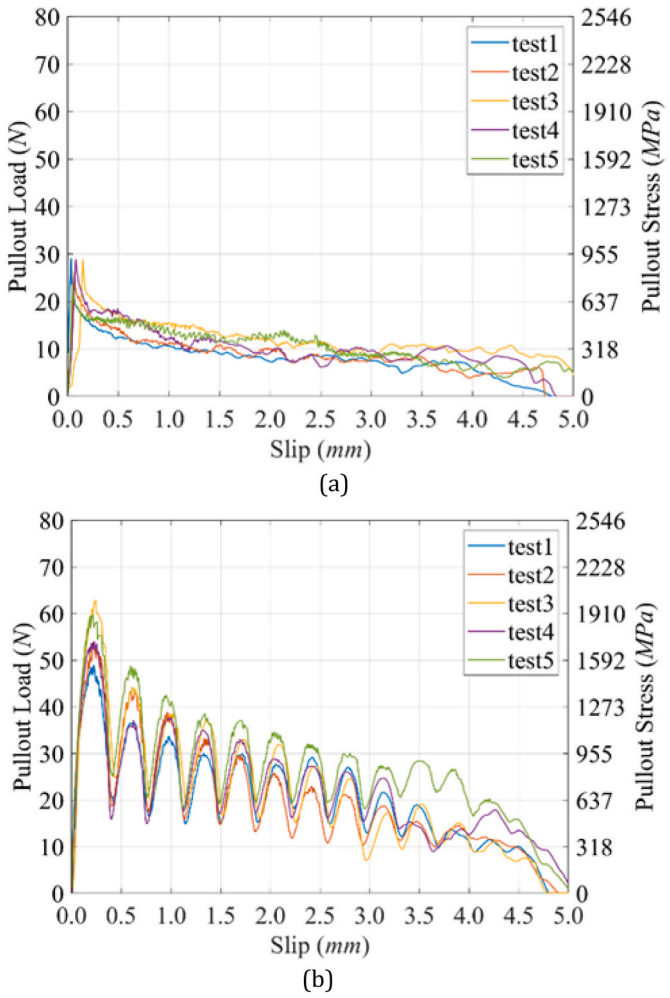

Fig. 3. Single fiber pull-out results: (a) smooth steel fiber; (b) striated steel fiber.

the bonded length, and interfacial load transfer gradually transitions from adhesion to friction within the debonded zone. The maximum pull-out load is reached when the bonded region is entirely exhausted and friction became the primary load-resisting mechanism.

In UHPC, the frictional resistance is strongly influenced by the dense matrix and the presence of hard, angular silica particles. Under the elevated normal pressures generated during pull-out, these particles act as micro-abrasives at the fiber–matrix interface, leading to longitudinal scratching and localized peeling of the brass coating on the steel fiber surface, as observed in Fig. 5. This abrasion progressively exposes the underlying steel and increases the effective surface roughness, thereby stabilizing and enhancing frictional resistance, consistent with observations reported by Wille and Naaman [23].

With continued slip, the embedded length decreases, reducing the available frictional interface. As a result, the pull-out load gradually declines to zero as frictional resistance is progressively lost.

5.1.2. *Striated steel fiber*

The pullout response of the striated fibers is discussed in light of the experimental data, the simulation results presented in the previous section, and the schematic diagram shown in Fig. 8, which synthesizes insights from both approaches. Like smooth fibers, the initial stage (Stage 0) is characterized by fully bonded behavior governed by chemical adhesion and the elastic stiffness of the UHPC matrix. As the adhesive bond is progressively overcome, interfacial debonding initiates and the response transitions to friction-dominated resistance.

As illustrated in Fig. 8, Stage 1 initiates when increasing slip causes the shear keys to bear against the edges of the shallow striations, resulting in a sharp increase in pullout resistance. Stage 2 begins once the mechanical interlock is overcome and the fiber slides past the striations, as observed in the simulation results. During this process, localized inelastic damage to the surrounding UHPC is inferred to occur, producing debris that accumulates within the striation voids (Fig. 4). Concurrently, frictional mechanisms contribute to resistance, as evidenced by the pronounced longitudinal scratches observed within the striated region and along the fiber surface outside the striations (Fig. 4). Based on the simulation results shown in Fig. 7, Stage 2 coincides with the peak pullout resistance.

Although degradation of the shear keys was not explicitly modeled, it is inferred that damage incurred during Stage 2 reduces the resistance offered to subsequent striations. Conversely, compaction of debris within the striation cavities as the fiber advances toward the next set of shear keys may partially counteract this degradation. As indicated by the simulation (Point C in Fig. 7), Stage 3 is characterized by elastic rebound effects, leading to a reduction in pullout resistance as each striation approaches and seats into the subsequent shear key. At this stage, the pullout load reaches a minimum level, comparable to that observed for smooth fibers.

The cycle then repeats in Stage 4, as continued pullout causes reengagement between the shear keys and the striations, returning the response to Stage 1. Stage 0 occurs only during the initial loading cycle, prior to complete debonding of the fiber. With progressive pullout, the number of engaged shear keys decreases, resulting in a proportional reduction in overall resistance. This repeating sequence of friction-controlled sliding and diminishing re-anchoring continues until all striations are extracted and the pullout load approaches zero.

5.2. *Analytical model development*

Fig. 9(a) shows a schematic description of the pullout behavior of the smooth steel fiber, where, as noted earlier, the response occurs in three stages, adhesion, followed by debonding/friction, then by friction. Fig. 9 (b) presents the averaged pull-out responses for both smooth and striated steel fibers on the same plot. It is clear from the figure that the smooth fiber response serves as an effective lower-bound envelope for the striated fiber's load-slip curve. Based on this observation, a new

Table 3
Pull-out test results for single steel fibers embedded in UHPC.

Index	Striated fiber				Smooth fiber			
	Max. Pull-out load (N)	Pullout energy, MPa-mm	Equivalent bond strength, MPa	Avg. bond strength, MPa	Max. Pull-out load (N)	Pullout energy, MPa-mm	Equivalent bond strength, MPa	Avg. bond strength, MPa
Test 1	48.97	99.16	0.79	15.59	29.05	39.32	0.31	9.25
Test 2	53.50	98.10	0.78	17.03	26.35	42.24	0.23	8.39
Test 3	62.79	106.5	0.85	19.99	26.81	58.92	0.47	9.17
Test 4	54.05	109.6	0.88	17.20	28.90	49.85	0.40	9.20
Test 5	59.74	134.3	1.07	19.01	23.55	52.24	0.42	7.49
Average (SD)	55.81 (5.46)	109.5 (14.67)	0.88 (0.12)	17.76 (1.74)	27.33 (2.24)	48.51 (7.87)	0.39 (0.096)	8.70 (0.76)

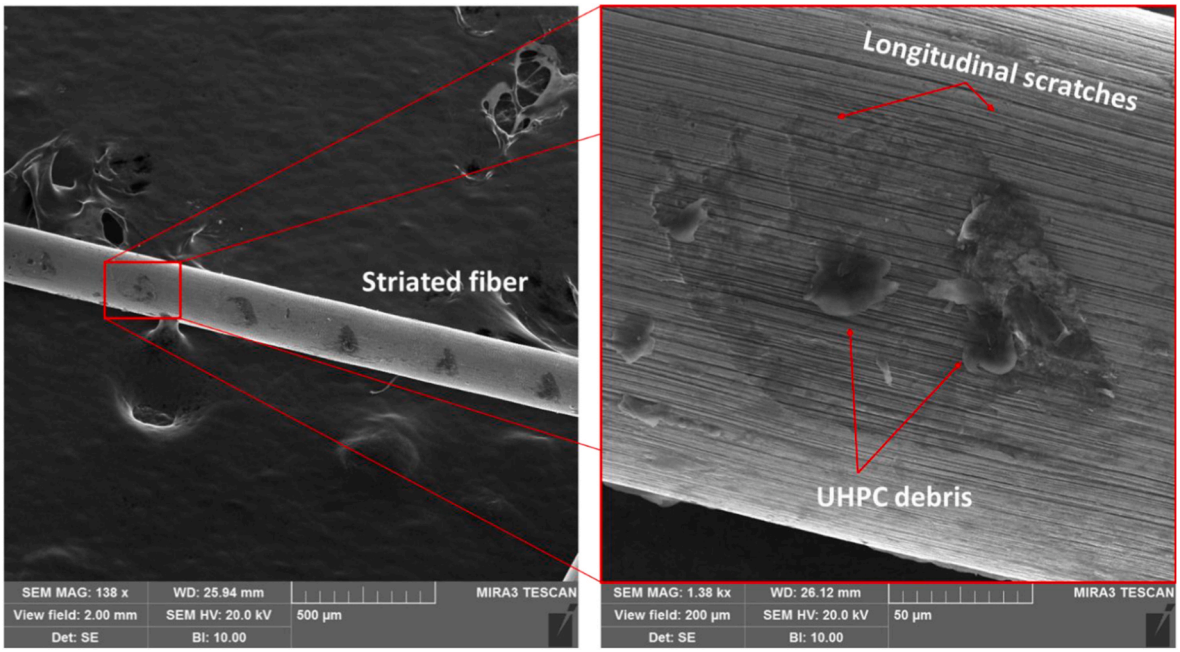

Fig. 4. SEM image of the striated fiber after the pull-out test.

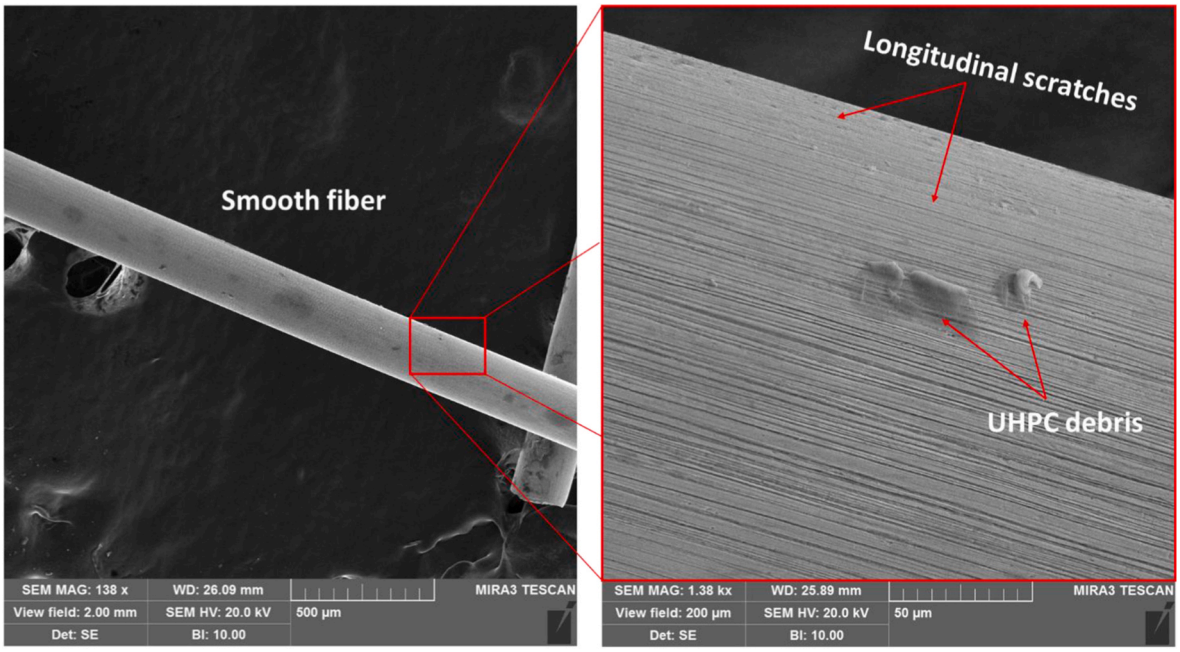

Fig. 5. SEM image of the smooth fiber after the pull-out test.

analytical model for striated fiber pull-out in UHPC is proposed as illustrated in Fig. 9(c). The parameter δ in Fig. 9(c) represents the spacing between successive anchorage events and matches the measured striation interval of 370 μm.

The analytical model for striated fiber (schematically illustrated in Fig. 9(c)) is developed under the following assumptions: (i) the steel fiber moves as a rigid body throughout the extraction process; (ii) the anchorage contribution is directly proportional to the number of striations still embedded; and (iii) after each anchorage event, the pull-out load decreases linearly to the smooth fiber envelope.

Consider a fiber with a diameter d_f, cross-sectional areas A, and elastic modulus of E, embedded in a UHPC matrix characterized by elastic modulus of E_m and Poisson's ratio ν_m, with an initial embedded length of L_E. A pull-out force P is applied at the fiber's free end, producing a slip displacement s, as illustrated in Fig. 9.

The bond stress-slip relation $\tau(s)$ for straight, smooth steel fibers is adopted from the model proposed by Zhan and Meschke [25]. For striated fibers, an additional constant shear frictional stress τ_f is introduced to account for the interaction between the UHPC matrix and the striation surfaces, as described in Section 5.1.2. The complete bond stress–slip relation is expressed as (see Fig. 9(c) for details):

$$\tau(s) = \begin{cases} Gs & \text{if } s \le s_0 \quad \text{(fully bonded stage)} \\ \tau_{max} & \text{if } s_0 < s \le s_1 \quad \text{(debonding stage)} \\ \tau_f & \text{if } s_i < s \le s_i + \alpha \quad \text{(anchoring stage)} \end{cases} \tag{3}$$

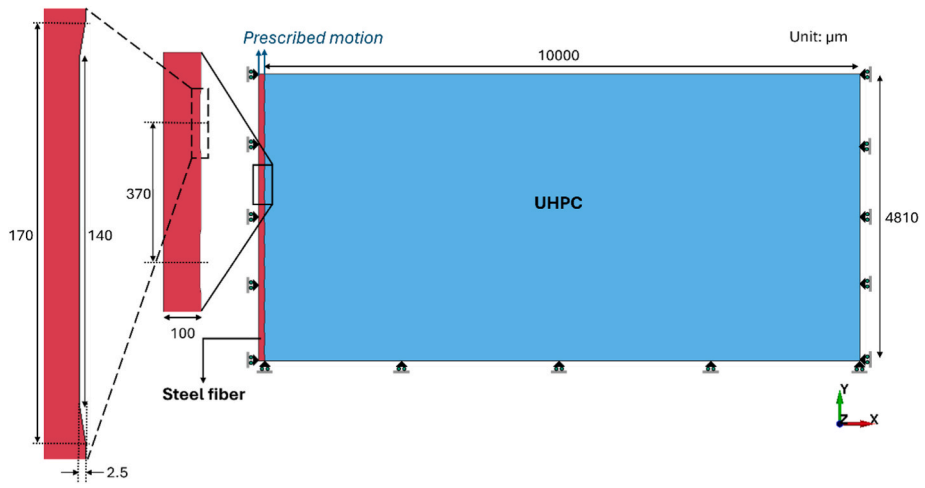

Fig. 6. Dimensions and boundary conditions of the axisymmetric steel fiber-UHPC model.

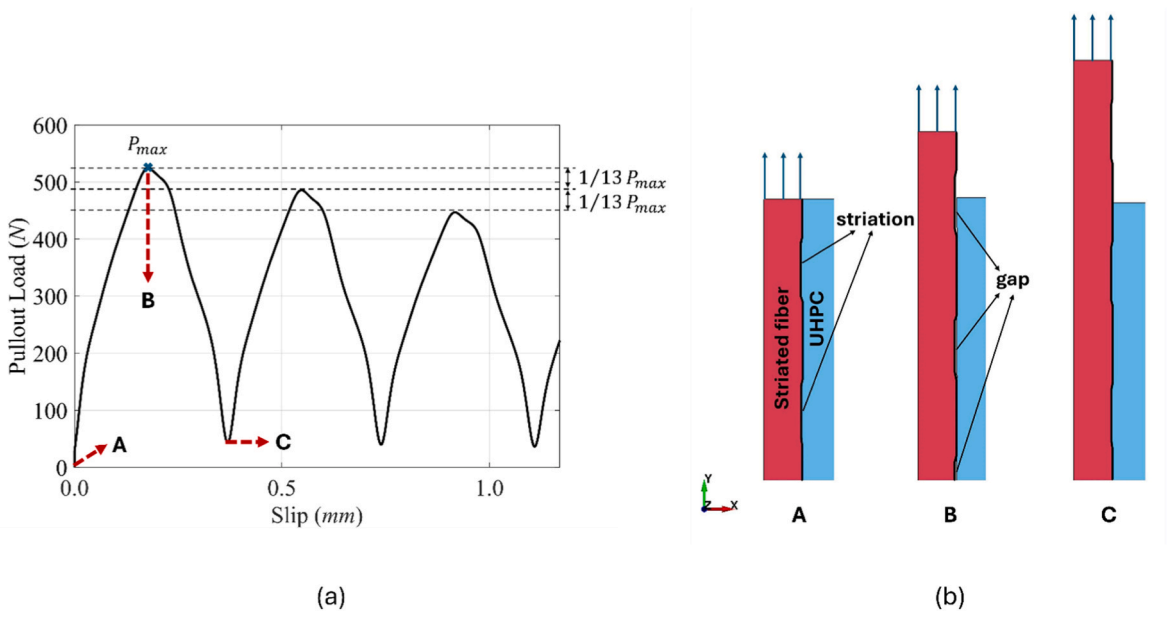

Fig. 7. (a) Load-slip relationship of the striated fiber from FE simulation, and (b) pullout phases of the striated fiber.

where τ presents the interfacial shear stress; s denotes the relative slip between the fiber and matrix; τ_{max} is the peak bond strength; s_i denotes the slip corresponding to the i-th anchorage stage; and α is the measured length of the striation (170 μm), i.e. the point at which the peak capacity is reached at the i-th anchorage stage.

The relative bond modulus G is defined [26] as:

$$G = \frac{E_m}{d_f(1+\nu_m)ln\left(\frac{R}{r}\right)} \tag{4}$$

where R/r is the ratio of matrix to fiber radius.

By incorporating the bond stress-slip relation and solving the force equilibrium and strain compatibility equations, the pull-out load-slip relation $P(s)$ can be derived for each mechanical stage as follows [27]:

i) Bonded stage [25] - Path AB in Fig. 9(c):

$$P = \frac{\pi d_f G\ tanh(\lambda L_E)}{\lambda} s \tag{5}$$

where $\lambda^2 = \frac{\pi dG}{AE}$.

ii) Debonding stage [25] - Path BC in Fig. 9(c):

$$P(L_d) = P_e + \pi d_f \tau_{max} L_d \tag{6}$$

$$s(L_d) = s_0 + \zeta\frac{\pi d_f \tau_{max} L_d^2}{2AE} + \frac{P_e L_d}{AE} \tag{7}$$

where L_d represents the debonded length, $P_e = \pi d_f \tau_{max}\ tanh(\lambda L_e)/\lambda$ denotes the axial force, and $L_e = L_E - L_d$ represents the remaining bonded length, respectively.

The factor ζ is introduced into the original equations proposed by Zhan and Meschke [25] to account for experimental uncertainties including imperfect fiber alignment during the casting, deviations from perfect straightness during fiber production, and residual surface oil from handling the fiber. A value of $\zeta = 2$ is adopted in this study, which leads to a slightly reduced initial stiffness in the load–slip response.

iii) Anchoring stage (applicable only to striated fibers) - Path CD in Fig. 9(c):

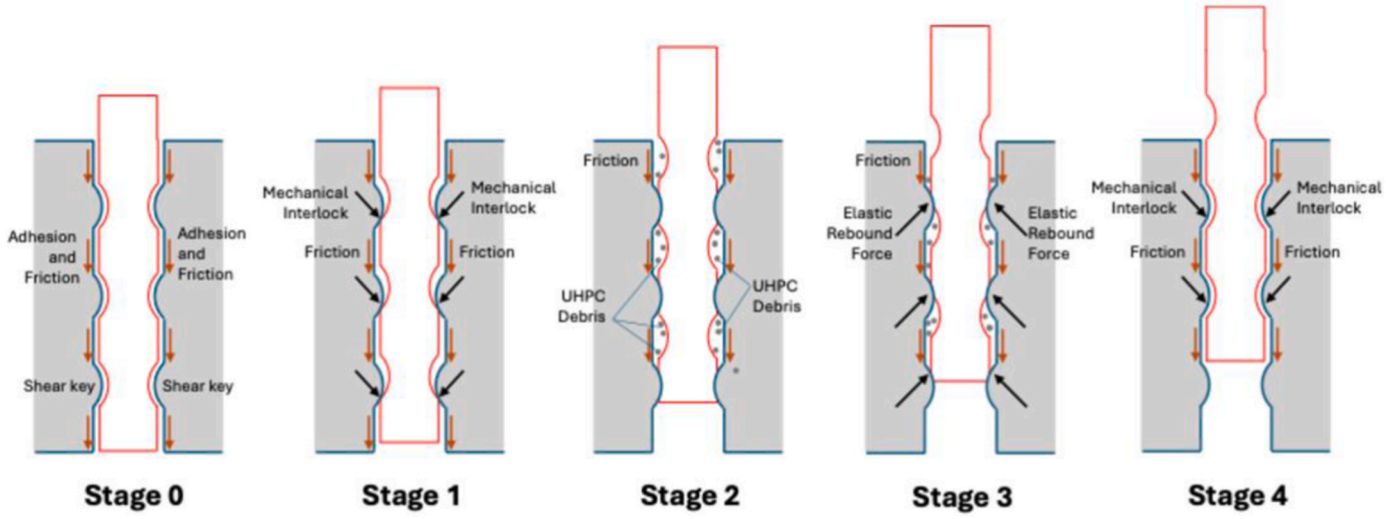

Fig. 8. Schematic showing envisioned pullout process.

$$P = \pi d_f \tau_{max} L_E + N d_f \tau_f (s - s_i) \tag{8}$$

where N is the number of embedded striations and τ_f is the constant friction bond stress. As implied by Equation (3), Equation (8) is valid in the region $s_i < s \leq s_i + \alpha$ and peaks at $s_i + \alpha$ for the i-th anchoring stage. The response drops linearly beyond $s_i + \alpha$ (Stages 2 and 3 discussed earlier) up until the start of the next anchoring stage (start of Stage 1). In the current fiber design, striations are formed on both sides of the fiber. Therefore, during the initial anchoring stage, 13 striations per side are fully engaged, resulting in a total of 26 striations in Equation (8).

iii) Anchoring stage (applicable only to striated fibers) - Path EF and subsequent anchoring paths in Fig. 9(c):

$$P = P_i + N d_f \tau_f (s - s_i) \tag{9}$$

where N is the number of embedded striations. P_i follows the load of the smooth fiber envelope, including $P_1 = \pi d_f \tau_{max} L_E$. The response drops linearly beyond $s_i + \alpha$ (Stages 2 and 3 discussed earlier) up until the start of the next anchoring stage (start of Stage 1).

iv) Pull-out sliding stage (applicable only to smooth fiber) (Zhan and Meschke 2014) - Path CEG in Fig. 9(c):

$$P = \pi d_f \cdot \tau \cdot (L_E - s + s_1) \tag{10}$$

where $\tau = \tau_0 + (\tau_{max} - \tau_0) exp\left[\frac{s_1 - s}{s_{ref}}\right]$ represents the decaying frictional stress during sliding, τ_0 is the asymptotic frictional stress, and s_{ref} governs the exponential decay rate of the frictional stress.

The proposed analytical model is evaluated by comparing its performance with the experimental results presented in Section 3.1. Although the model is built upon the conceptual framework introduced by Zhan and Meschke [25], the key interfacial parameters, such as the maximum bond stress $\boldsymbol{\tau_{max}}$ and asymptotic friction stress $\boldsymbol{\tau_0}$, are independently calibrated using the present experimental data to reflect the distinct behavior of UHPC matrix (compressive strength >150 MPa) compared to conventional cementitious matrices (compressive strength = 36.5 MPa). For instance, a substantially higher value of $\boldsymbol{\tau_0}$ is adopted in this study because most smooth steel fibers exhibit end deformations (flattening) caused by the cutting process, which contributes a constant anchorage force during pull-out that abruptly drops upon complete fiber extraction, particularly in densely packed matrices such as UHPC [23]. The reference slip $\boldsymbol{s_{ref}}$ is adopted from Zhan and Meschke's original formulation. All parameters used for the model are summarized in Table 4.

Fig. 10(a) compares the model predictions with the measured pull-out load–slip responses for smooth steel fibers. The model captures the overall behavior reasonably well, including the initial stiffness, peak load, and post-peak softening, demonstrating its ability to represent the bond–slip mechanisms under monotonic pull-out conditions. However, some discrepancies are observed. In the debonding stage, the model exhibits a stiffer response than the experimental data, likely due to aforementioned experimental uncertainties. Additionally, during the sliding phase, deviations may stem from the original formulation's assumptions about interfacial behavior between smooth fibers and conventional cementitious matrices, which may not fully capture the more complex frictional interactions present in the densely packed UHPC matrix.

Fig. 10(b) compares the computed and experimental pull-out responses for specimens incorporating striated fibers. The model is able to successfully replicate key features of the response, including the load peaks from striation engagement and the transition to sliding resistance, demonstrating its capacity to capture the effects of the surface striations. Clearly, the proposed model effectively represents the observed response, capturing both frictional and mechanical contributions to fiber pull-out resistance. Obviously, the proposed model was based upon only one set of test data and therefore its effectiveness across different fiber geometries and matrix types needs to be evaluated through further research.

6. Conclusion

This study provides the first comprehensive investigation into the pull-out behavior and interfacial mechanisms of striated steel fibers embedded in ultra-high performance concrete (UHPC). Combining single-fiber pull-out experiments, finite element (FE) simulations, and analytical modeling, the research elucidates how micrometer-scale surface striations fundamentally alter the load-transfer mechanism between steel fibers and UHPC. The key findings can be summarized as follows:

1. Striated steel fibers exhibited a repetitive sequence of load peaks and drops associated with successive engagement and release of the striations. Each cycle is characterized by frictional sliding and intermittent re-engagement of the fiber with the UHPC matrix, accompanied by inferred localized damage and debris formation within the striation region. The resulting sawtooth pullout response, which has not been reported for conventional smooth or deformed

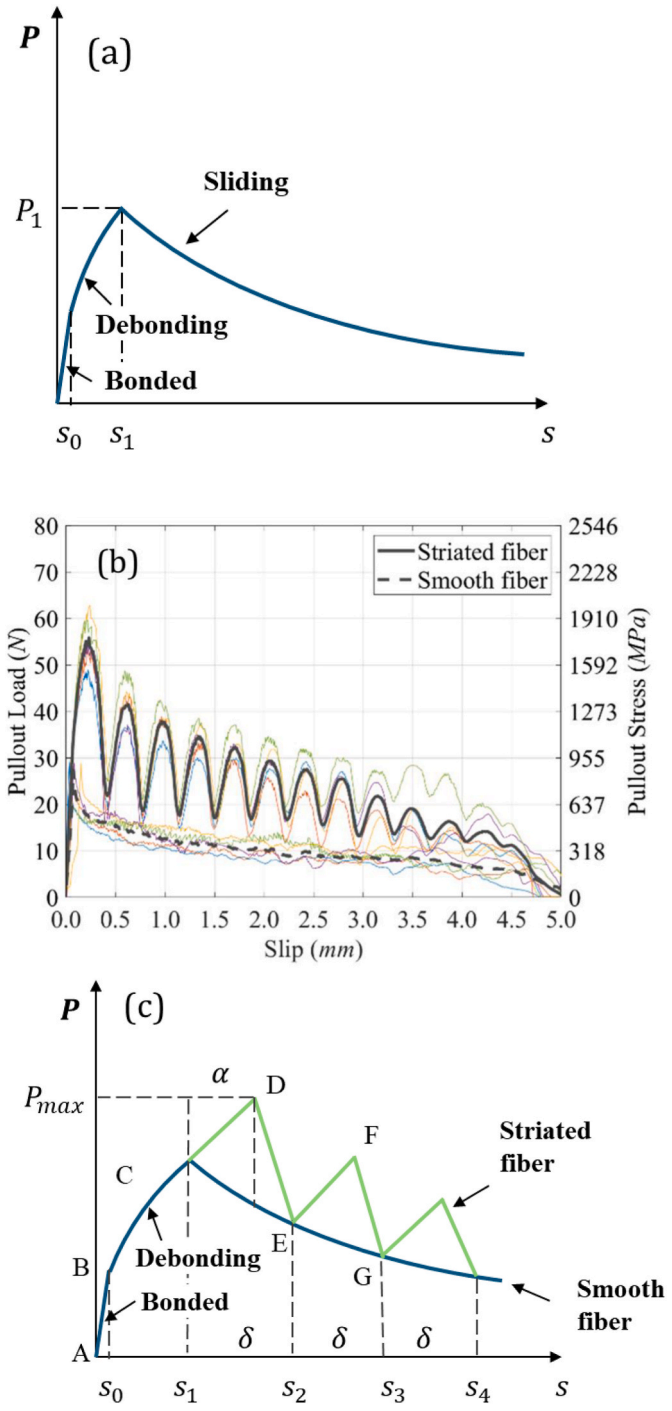

Fig. 9. (a) Stages of pull-out behavior in smooth fiber in UHPC; (b) averaged experimental pull-out response of steel fibers in UHPC; (c) stages of pull-out behavior in striated fiber in UHPC.

steel fibers, highlights a distinct interaction mechanism enabled by the striated geometry.

2. On average, striated fibers achieved 104% higher maximum pull-out load and 126% greater equivalent bond strength than smooth fibers. This improvement is attributed to the formation of localized shear keys within the striations and increased frictional resistance at the fiber-matrix interface. Such improvements in interfacial efficiency suggest that comparable or improved composite-level performance may be achievable with reduced steel fiber dosage, offering potential benefits in material economy and sustainability of UHPC systems.

Table 4
Parameters used for modeling the pull-out behavior of smooth and striated steel fibers.

Parameter	Value
Matrix and fiber	
Elastic modulus of matrix E_m	45.0 GPa
Poisson's ratio of matrix ν_m	0.2
Elastic modulus of fiber E	210 GPa
Interaction	
Embedment length L_E	5 mm
Matrix-fiber size ratio R/r	125
Bond strength τ_{max}	9.0 MPa
Asymptotic frictional stress τ_0	4.5 MPa
shear frictional stress τ_f	27.0 MPa
Reference slip s_{ref}	0.25 mm

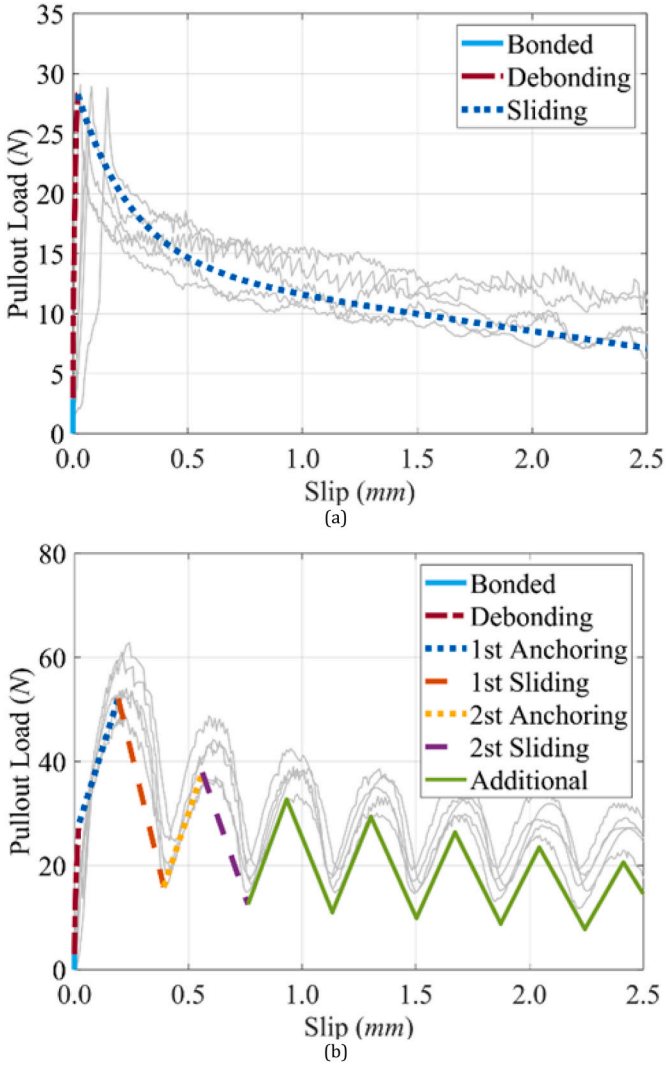

Fig. 10. Schematic representation of the analytical model for pull-out behavior in UHPC: (a) smooth straight fiber; (b) striated fiber (Note: Gray lines denote the corresponding experimental pull-out responses.).

3. SEM imaging revealed UHPC residues retained within the striation grooves, indicating material retention and abrasive interaction during pullout. The finite element simulations reproduced the characteristic oscillatory load–slip response and provided qualitative insight into the sequence of interfacial engagement, sliding, and re-

engagement mechanisms that underlie the experimentally observed behavior.

4. An analytical model was proposed to represent both frictional and anchorage contributions to pull-out resistance. Despite its simplicity, the model reproduced the key trends observed experimentally, supporting the mechanistic interpretation of striation engagement.

This study provides a mechanistic interpretation of the pull-out behavior of striated steel fibers in UHPC by clarifying the roles of micrometer-scale surface geometry in adhesion, friction, and mechanical interlock. However, the investigation was limited to a single striated fiber geometry, embedment length, and UHPC matrix composition. Accordingly, the results cannot be directly generalized to other striation configurations, fiber orientations, or matrix strengths.

The proposed analytical model was developed as a first-order framework calibrated to the tested system to capture the essential features of the multi-stage pull-out response. While it reproduces the overall trends observed experimentally, it does not explicitly account for progressive matrix damage, local crushing, or debris compaction at the fiber-matrix interface. Furthermore, as the current formulation is calibrated to specific fiber and embedment configurations, its predictive capability across different geometries requires further validation through systematic experimental and parametric studies.

Future studies should extend this work to systematically examine the influence of striation geometry (e.g., depth, spacing, and profile), embedment length, and fiber orientation on pull-out behavior, supported by expanded experimental programs and refined numerical modeling. Incorporating quantitative microstructural characterization alongside mechanical testing would further improve understanding of interfacial damage evolution and facilitate the development of more general design guidelines for striated steel fibers in UHPC. Because the number of engaged striations is governed by the embedment length, the number of load peaks is expected to scale with the number of active striations; however, systematic experimental verification across different embedment lengths remains a subject for future study.

CRediT authorship contribution statement

Sukhoon Pyo: Writing – original draft, Investigation, Formal analysis, Conceptualization. **Zhengye Tang:** Writing – review & editing, Visualization, Formal analysis, Data curation. **Min-Chun Han:** Writing – review & editing, Visualization, Software, Methodology, Investigation, Formal analysis. **Sherif El-Tawil:** Writing – review & editing, Supervision, Resources, Project administration, Formal analysis, Conceptualization.

Declaration of competing interest

The authors declare the following financial interests/personal relationships which may be considered as potential competing interests: The striated steel fibers used in this study were manufactured by HiPer Fiber, Inc. and provided to the University of Michigan for use in this research. The senior author, Sherif El-Tawil, holds a significant ownership interest in HiPer Fiber, Inc. The underlying patent for the fiber design is owned by the University of Michigan and is exclusively licensed to HiPer Fiber, Inc. The conflict of interest arising from these relationships is managed by the Conflict of Interest Office at the University of Michigan.

Acknowledgement

This research was supported jointly by the University of Michigan and the Michigan Department of Transportation (*MDOT*). Any opinions, findings, conclusions, and recommendations expressed in this paper are those of the authors and do not necessarily reflect the views of the sponsors. The first author was supported by the National Research Foundation of Korea (NRF) grant funded by the Korea government (MSIT) (No. RS-2023-00212366 and RS-2024-00399324).

Data availability

Data will be made available on request.

References

[1] J.M. Alwan, A.E. Naaman, W. Hansen, Pull-out work of steel fibers from cementitious composites: analytical investigation, Cement Concr. Compos. 13 (4) (1991) 247–255.
[2] A.E. Naaman, Toughness, ductitlity, surface energy and deflection-hardening FRC composites, in: Proc. JCI Int. Workshop on Ductile Fiber Reinforced Cementitious Composites (DFRCC), 2002, 2002.
[3] A.E. Naaman, Engineered steel fibers with optimal properties for reinforcement of cement composites, J. Adv. Concr. Technol. 1 (3) (2003) 241–252.
[4] F. Isla, G. Ruano, B. Luccioni, Analysis of steel fibers pull-out. Experimental study, Constr. Build. Mater. 100 (2015) 183–193.
[5] S. Pyo, K. Wille, S. El-Tawil, A.E. Naaman, Strain rate dependent properties of ultra high performance fiber reinforced concrete (UHP-FRC) under tension, Cement Concr. Compos. 56 (2015) 15–24.
[6] L. Ke, X. Wu, Z. Feng, C. Li, D.Y. Yoo, B. Yan, Enhancing interfacial bond performance of steel fibers embedded in ultra-high-performance concrete through surface dezincification and chelation treatments, Cement Concr. Compos. 160 (2025) 106062.
[7] D.Y. Yoo, N. Banthia, Y.S. Yoon, Recent development of innovative steel fibers for ultra-high-performance concrete (UHPC): a critical review, Cement Concr. Compos. 145 (2024) 105359.
[8] S. Kim, S. Choi, D.Y. Yoo, Surface modification of steel fibers using chemical solutions and their pullout behaviors from ultra-high-performance concrete, J. Build. Eng. 32 (2020) 101709.
[9] T. Liu, H. Wei, A. Zhou, D. Zou, H. Jian, Multiscale investigation on tensile properties of ultra-high performance concrete with silane coupling agent modified steel fibers, Cement Concr. Compos. 111 (2020) 103638.
[10] Y. Zhou, X. Zhong, C. Zhao, T. Luo, K. Tian, Y. Li, Study on the strengthening and toughening mechanism of ultra-high-performance concrete through hydrogen peroxide activation and corrosion of steel fibers with surface-anchored carbon nanotubes, Constr. Build. Mater. 501 (2025) 144359.
[11] J. Tian, Y. Li, G. Yang, M. Su, Z. Yang, Silane-nanoSiO2 composite surface modification of steel fibres: a multiscale experimental study of fibre-UHPC interfaces, Compos. B Eng. (2025) 112999.
[12] S. Abdallah, M. Fan, D.W. Rees, Bonding mechanisms and strength of steel fiber–reinforced cementitious composites: overview, J. Mater. Civ. Eng. 30 (3) (2018) 04018001.
[13] D.J. Kim, S. El-Tawil, A.E. Naaman, Loading rate effect on pullout behavior of deformed steel fibers, ACI Mater. J. 105 (6) (2008) 576.
[14] Y. Deng, Z. Zhang, C. Shi, Z. Wu, C. Zhang, Steel fiber–matrix interfacial bond in ultra-high performance concrete: a review, Engineering 22 (2023) 215–232.
[15] D.J. Kim, A.E. Naaman, S. El-Tawil, High performance fiber reinforced cement composites with innovative slip hardending twisted steel fibers, Int. J. Concr. Struct. Mater. 3 (2) (2009) 119–126.
[16] Y.S. Tai, S. El-Tawil, Computational investigation of twisted fiber pullout from ultra-high performance concrete, Constr. Build. Mater. 222 (2019) 229–242.
[17] S. El-Tawil, *High Bond Steel Fibers for Ultra High-Performance Concrete (UHPC)* (No. NCHRP IDEA Project 235), 2022.
[18] Z. Tang, M.C. Han, S. El-Tawil, S. Pyo, Performance and implications of cost-effective natural sand substitutes for quartz in ultra-high performance concrete, Constr. Build. Mater. 496 (2025) 143759.
[19] S. El-Tawil, M.A. Saqif, W. Hazelton, J. Winckler, M. Clark, Construction of a short-span UHPC bridge: Cost considerations and lessons learned, Concr. Int. 47 (2) (2025).
[20] AASHTO, Guide specification for structural design with ultra-high performance concrete. March 2024, American Association of State Highway Transportation Officials, 555 12th Street NW, Suite 1000, Washington, DC 20004, first ed., 2024.
[21] S. El-Tawil, Y.S. Tai, J.A. Belcher II, D. Rogers, Open-recipe ultra-high-performance concrete, Concr. Int. 42 (6) (2020) 33–38.
[22] K. Wille, A.E. Naaman, Pullout behavior of high-strength steel fibers embedded in ultra-high-performance concrete, ACI Mater. J. 109 (4) (2012).
[23] K. Wille, A.E. Naaman, Effect of ultra-high-performance concrete on pullout behavior of high-strength brass-coated straight steel fibers, ACI Mater. J. 110 (4) (2013) 451.
[24] B.A. Graybeal, Material property characterization of ultra-high performance concrete. Federal Highway Administration (FHWA), Turner-Fairbank Highway Research Center, 2006. McLean, VA. Report No. FHWA-HRT-06-103.
[25] Y. Zhan, G. Meschke, Analytical model for the pullout behavior of straight and hooked-end steel fibers, J. Eng. Mech. 140 (12) (2014) 04014091.
[26] J. Kullaa, Dimensional analysis of bond modulus in fiber pullout, J. Struct. Eng. 122 (7) (1996) 783–787.
[27] F. Deng, X. Ding, Y. Chi, L. Xu, L. Wang, The pull-out behavior of straight and hooked-end steel fiber from hybrid fiber reinforced cementitious composite: experimental study and analytical modelling, Compos. Struct. 206 (2018) 693–712.